Chapter 4

Mixed ligand metal complexes of quinolone antibacterials: synthesis, characterization, interaction with DNA and cytotoxicity studies.

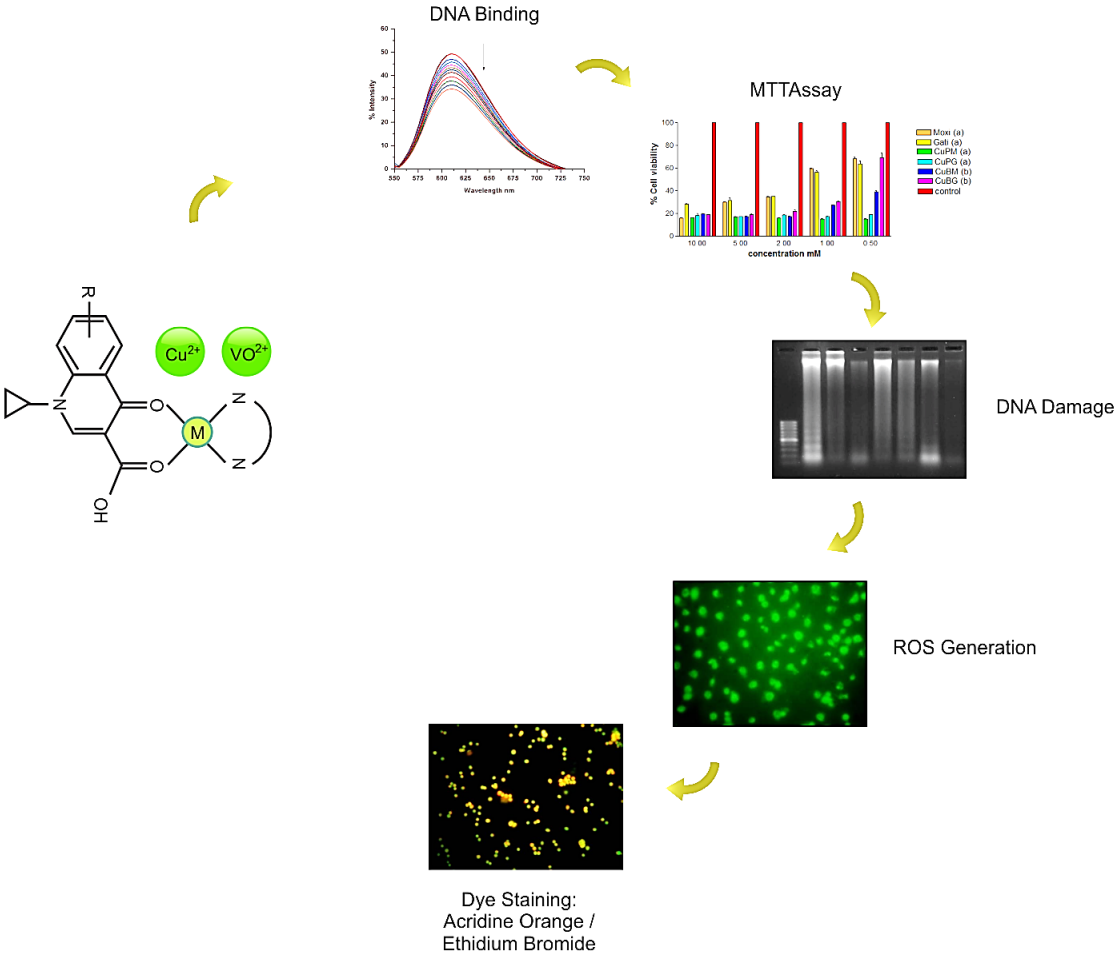

4.1 Introduction

Gatifloxacin(1-cyclopropyl-1,4-dihydro-6fluoro-8-methoxy-7-(3-methyl-1-piperazinyl)-4-oxo-3-quinolinecarboxylic acid, GFL) is a 3rd generation fluoroquinolone with a broad spectrum of antibacterial activity including activity against penicillin resistant streptococcus pneumonia. Like other quinolones, gatifloxacin works by inhibiting DNA gyrase, a bacterial DNA topoisomerase II. This action results in inhibition of bacterial growth.

1,10-Phenanthroline(phen) and 2,2'bipyridyl (bpy) are classic chelating bidentate ligands for transition metal ions that have played important roles in the development of coordination chemistry [1,2]. Phen is a rigid planar, hydrophobic, electron-deficient heteroaromatic system whose nitrogen atoms are placed to act cooperatively in cation binding. These structural features determine its coordination ability toward metal ions. Since the discovery of 2,2'-bipyridine in nineteenth century it has been used extensively as metal chelating ligand due to its robust redox stability and ease of functionalization. [3,4].Taking advantages of these structural features (planarity, rigidity and hydrophobicity) phen and bpy derivatives and their metal complexes have been studied, as intercalating or groove binding agents for DNA and RNA [2,4,5].

Copper is a physiologically relevant metal that plays an important role in many biological processes and exhibits considerable biochemical action either as an essential trace metal or as a constituent of various exogenously administered compounds in humans [6]. Since the discovery, in 1979 [7], that copper ions when complexed to 1,10-phenanthroline were capable of DNA cleavage, its biological activity has been the subject of numerous studies [8]. Current interest in copper complexes comes from their potential use as antimicrobial, antiviral, anti-inflammatory or as antitumor agents, due to their biological roles and synergetic activity with drugs [9].

Vanadium is a widespread element in the environment and it is present at trace concentrations in biological systems [10]. It can form a great variety of compounds in different oxidation states (III, IV, and V). Vanadium (IV) is easily oxidized to vanadium (V) under physiological conditions, and vanadium (V) species are found as vanadate anions in biological systems [11]. For many years vanadium have attracted the scientific interest due to the complexity of its chemical behaviour, different oxidation states and the great versatility of coordination sphere around the metal centre [12,13]. It has been reported that this metal can regulate cell growth. It behaves as a growth factor mimetic agent [14] and promotes morphological alterations in the cells [15].

In some cases it also induces anti-metastatic behaviour, decreasing cell spreading and adhesion to the extracellular matrix. On the other hand, it has also been demonstrated that vanadium compounds induce the generation of reactive oxygen species (ROS) which play an important role in their adverse biological effects. Previously reported studies have shown that vanadium compounds promote apoptosis and cause cell death by increasing ROS levels and disturbance of the redox status, especially by alteration of mitochondrial functions in the cells [16]. Studies with oxidovanadium(IV) complexes have demonstrated that some compounds cause substantial single strand breaks in DNA and produce lipid peroxidation [17].

Various organically chelated vanadium compounds are more potent to facilitate pharmacological actions than the simple vanadium salts [18]. This is attributed, among other factors, to the poor absorption of some vanadium species in the gastrointestinal tract. For this reason, the use of organic ligands would enhance the lipophilicity of vanadium, increasing the gastrointestinal absorption, and thereby decreasing the dose of vanadium required to produce its biological or pharmacological effects [19]. In this sense, the synthesis of vanadium complexes with ligands that hold multiple donor atoms is of considerable interest in vanadium biochemistry and in relation to their potential therapeutic applications.

The present study deals with the effects of ternary copper and vanadium complexes of moxifloxacin (MFL) and gatifloxacin (GFL) with 1, 10-phenanthroline and 2, 2'-bipyridyl as ancillary ligand on plasmid DNA as a model for the interactions of these compounds with cellular DNA. We have investigated the effects of the synthesised complexes against the A-549 (lung cancer) cell lines. We report herein the action of these compounds on the proliferation of this tumoral cell line and the putative mechanisms involved in their antiproliferative effects. In particular, we focused our investigation on the role of oxidative stress, its effects on cytotoxicity, as well as on the morphological transformations and apoptosis. The antibacterial activity of the complexes has been evaluated by determining the zone of inhibition (ZI) against four microorganisms.

4.2 (a) General synthesis of complexes (1-4)

The compounds were synthesized as shown in Scheme 4.1. A methanolic solution of the fluoroquinolone (GFL/MFL) (1.0 mmol) in presence of KOH (1.0 mmol) was added to an aqueous solution of $CuCl_2.5H_2O$ (1.0 mmol) and stirred for 30 min, followed by addition of a methanolic solution of the neutral bidentate ligand (phen/bpy) (1.0 mmol). The pH was adjusted to 6.2 using dilute solution of KOH. The resulting solution was refluxed for 2 h. The green microcrystalline product obtained was washed with ether and dried. The complexes were characterized by physico-chemical and spectroscopic methods and the general composition of the complexes was derived as [Cu(A)(L)Cl]. $5H_2O$, where A= MFL/GFL and L= phen/bpy, from the data obtained.

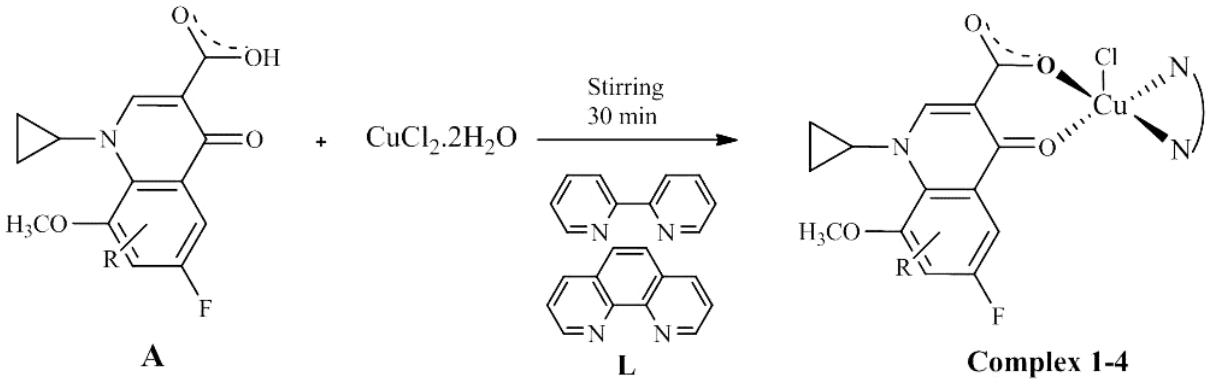

A = Moxifloxacin/ Gatifloxacin

L= bipyridyl / 1,10-Phenanthroline

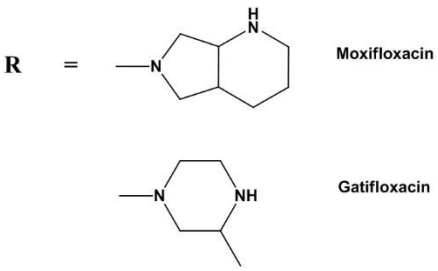

. **Scheme 4.1**

4.2 (b) General synthesis of complexes (5-8)

The compounds were synthesized as shown in Scheme 4.2. A methanolic solution of fluoroquinolone (GFL/MFL) (1.5 mmol) in presence of sod. methoxide (1.5 mmol) was added to an aqueous solution of $VOSO_4.2H_2O$(1.5 mmol) and stirred for 30 min, followed by addition of a methanolic solution of the neutral bidentate ligand (phen/bpy) (1.5 mmol). The pH was adjusted to 6.2 using dilute solution of sod. methoxide. The resulting solution was refluxed for 2 h on a steam bath. The microcrystalline product of green colour obtained was washed with ether and dried. The complexes were characterized by physico-chemical and spectroscopic methods and the general composition of the complexes was derived as [VO(A)(L)]. $0.5SO_4$ $.2H_2O$ from the data obtained since no single crystals of the complexes suitable for the X-ray determination could be isolated.

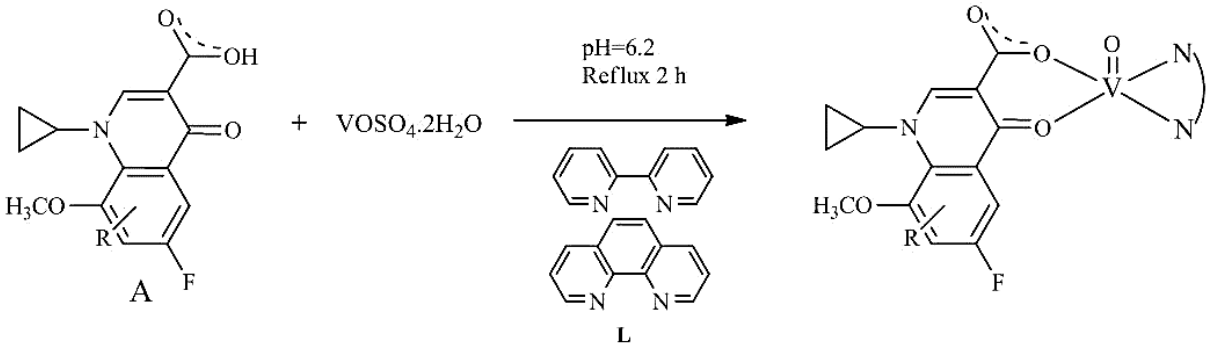

A = Moxifloxacin/ Gatifloxacin

L= bipyridyl / 1,10-Phenanthroline

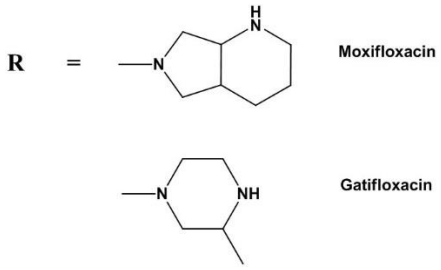

Scheme 4.2

4.3 Physicochemical data of the synthesized complexes

A. [Cu(MFL)(phen)Cl].5H_2O **(1)**

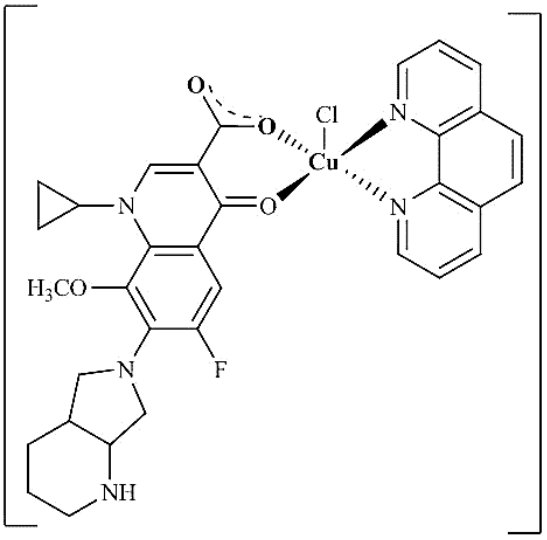

Yield: 71%
Molecular weight: 680.14 g/mol
Molecular formula: $C_{33}H_{32}ClCuFN_5O_4$
Calc. (%): C, 58.23; H, 4.74; N, 10.29; Cu, 9.40
Found (%):C, 58.54; H, 4.82; N, 10.56; Cu, 9.45
λ_{max}:295, 370, 410, 634 nm.
ESI-MS [MeOH, *m/z*]: 680.4 [M^+]
IR: 1591 (COO_{asym}), 1386(COO_{sym}), 1627 $(C=O)_{ketone}$

B. [Cu(MFL)(bpy)Cl].5H_2O **(2)**

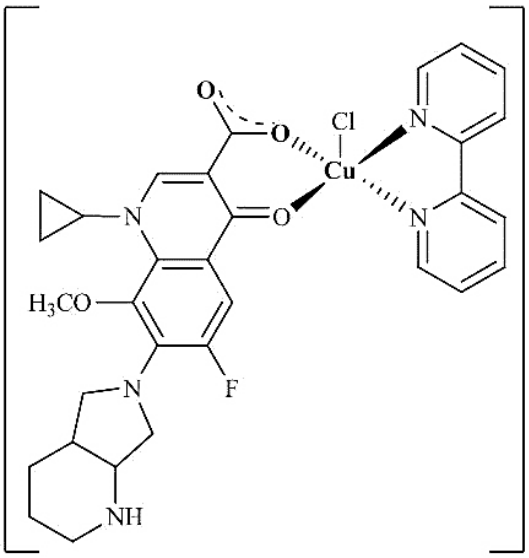

Yield: 69%
Molecular weight: 656.14 g/mol
Molecular formula: $C_{31}H_{32}ClCuFN_5O_4$
Calc. (%): C, 56.89; H, 4.88; N, 10.72; Cu, 9.78
Found (%):C, 56.60; H, 4.91; N, 10.72; Cu, 9.78
λ_{max}:289, 360, 420, 638 nm.
ESI-MS [MeOH, *m/z*]: 655.0[M-1]
IR: 1587 (COO_{asym}), 1376 (COO_{sym}), 1634 $(C=O)_{ketone}$

C. [Cu(GFL)(phen)Cl].5H_2O **(3)**

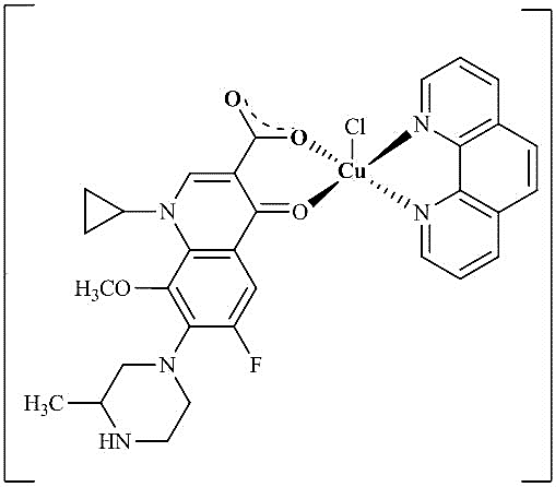 . $5H_2O$	Yield: 71% Molecular weight: 653.13 g/mol Molecular formula: $C_{31}H_{30}ClCuFN_5O_4$ Calc. (%): C, 56.54; H, 4.65; N, 10.75; Cu, 9.75 Found (%):C, 56.54; H, 4.65; N, 10.70; Cu, 9.78 λ_{max}:299, 360, 420, 638 nm. ESI-MS [MeOH, *m/z*]: 653.4 [M^+] IR: 1598 (COO_{asym}), 1385(COO_{sym}), 1684 $(C=O)_{ketone}$

D. [Cu(GFL)(bpy)Cl].5H_2O **(4)**

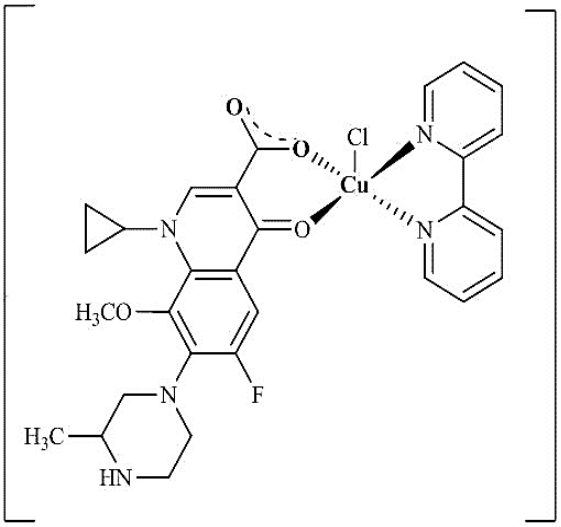 . $5H_2O$	Yield: 65% Molecular weight: 630.58 g/mol Molecular formula: $C_{29}H_{32}ClCuFN_5O_4$ Calc. (%): C, 55.56; H, 4.89; N, 11.23; Cu, 10.0 Found (%):C, 55.24; H, 4.80; N, 11.11; Cu, 10.08 λ_{max}:300, 358, 417, 627 nm. ESI-MS [MeOH, *m/z*]: 629.13[M-1] IR: 1589 (COO_{asym}), 1377(COO_{sym}), 1683 $(C=O)_{ketone}$

E. [VO(MFL)(phen)] 0.5 SO_4. $2H_2O$ **(5)**

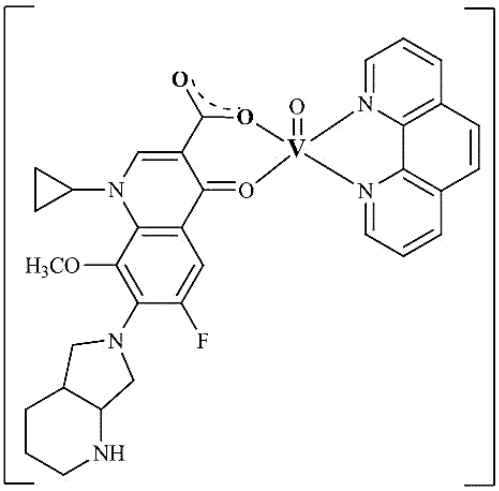 $0.5\ SO_4.\ 2H_2O$	Yield: 72% Molecular weight: 647.18 g/mol Molecular formula:$C_{33}H_{32}FN_5O_5V$ Calc. (%): C, 61.11; H, 4.97; N, 10.8; V,7.85, Found (%): C, 60.89; H, 4.91; N, 10.67; V, 7.76 λ_{max}:286, 337, 435, 522(sh), 743 nm. ESI-MS [MeOH, *m/z*]: 646.6[M-1] IR: 1572 (COO_{asym}), 1370(COO_{sym}), 1632 $(C=O)_{ketone}$, 954(V=O)

F. [VO(MFL)(bpy)] 0.5 SO_4. $2H_2O$ **(6)**

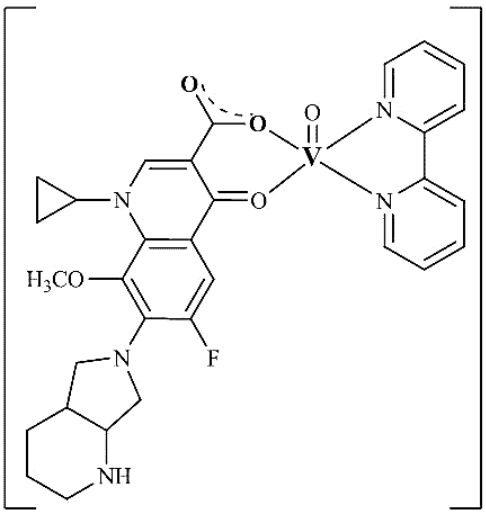 $0.5\ SO_4.\ 2H_2O$	Yield: 68% Molecular weight: 623.18 g/mol Molecular formula: $C_{31}H_{32}FN_5O_5V$ Calc. (%): C, 59.62; H, 5.16; N, 11.21; V, 8.16 Found (%):C, 58.23; H, 4.98; N, 11.17; V, 8.10 λ_{max}:288, 337, 437, 522(sh), 719 nm. ESI-MS [MeOH, *m/z*]: 626.6 [M+3] IR: 1581(COO_{asym}), 1365(COO_{sym}), 1627 $(C=O)_{ketone}$, 964(V=O)

G. [VO(GFL)(phen)] 0.5 SO_4. $2H_2O$ **(7)**

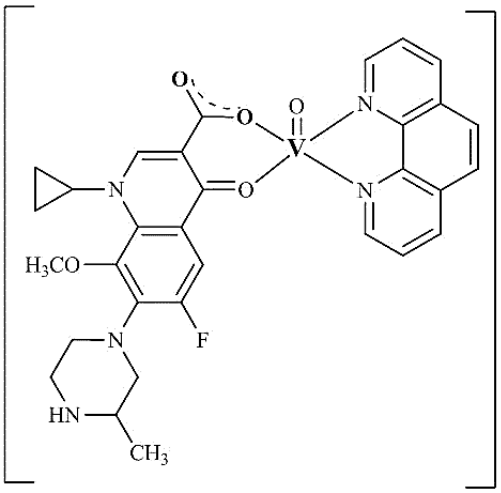

$0.5\ SO_4.\ 2H_2O$

Yield: 75%
Molecular weight: 621.17 g/mol
Molecular formula: $C_{31}H_{32}FN_5O_5V$
Calc. (%): C, 59.81; H, 4.86; N, 11.25; V, 8.18
Found (%):C, 59.25; H, 4.80; N, 11.11; V, 8.10
λ_{max}:287, 332, 402,526(sh), 748 nm.
ESI-MS [MeOH, *m/z*]: 621.8 [M^+]
IR: 1578 (COO_{asym}), 1342(COO_{sym}), 1624 $(C=O)_{ketone}$, 950(V=O)

F. [VO(GFL)(bpy)] 0.5 SO_4. $2H_2O$ **(8)**

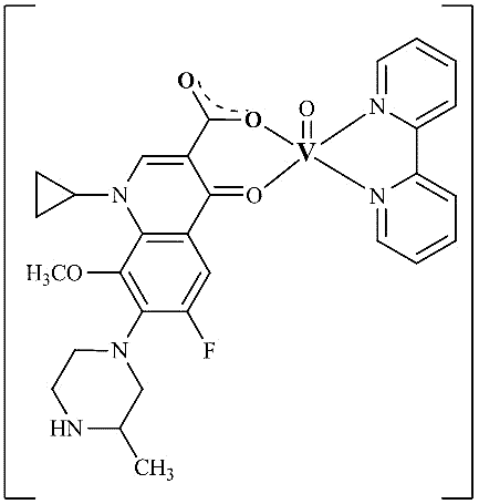

$0.5\ SO_4.\ 2H_2O$

Yield: 64%
Molecular weight: 597.8 g/mol
Molecular formula: $C_{29}H_{30}FN_5O_5V$
Calc. (%): C, 58.20; H, 5.05; N, 11.70; V, 8.51
Found (%):C, 58.42; H, 5.19; N, 11.70; V, 8.38
λ_{max}:288, 330, 408, 526(sh),724 nm.
ESI-MS [MeOH, *m/z*]: 597.6 [M^+]
IR: 1565 (COO_{asym}), 1328(COO_{sym}), 1635 $(C=O)_{ketone}$, 962(V=O)

4.4 Results and discussions

4.4.1 Synthesis and general properties

The metal complexes were prepared in high yields (~70%) by the reaction of the fluoroquinolones (MFL/GFL) with the corresponding metal salts ($CuCl_2$/$VOSO_4$) and N-N donor ligands (phen/bpy) in the ratio 1:1:1 in methanolic solution. The complexes were characterized by various spectroscopic and analytical techniques.All the complexes displayed the expected molecular ion peaks in their ESI-MS spectrum.

The infrared spectra of all the synthesized complexes exhibited major changes as compared to the spectra of free ligands. The strong bands at ~1712 and 1623 cm^{-1} in the spectrum of moxifloxacin were assigned to pyridone carbonyl and carboxyl stretches. The same appeared at 1713 and 1625 cm^{-1} in the spectrum of gatifloxacin (Table 4.1). In the complexes, the $\upsilon(COO)_{carboxylate}$ stretching frequency has been replaced by two very strong characteristic bands in the range of 1565-1598 cm^{-1} and 1321-1398 cm^{-1}, assigned respectively to υ(O-C-O) antisymmetric and symmetric stretching vibrations. Additionally, $\upsilon(C=O)_{ket}$ was shifted from 1712 cm^{-1} (MFL) and 1731 cm^{-1} (GFL) up to 1627–1684 cm^{-1} upon bonding (Fig.4.1). The values of $\Delta[\upsilon_{asym(COO)} - \upsilon_{sym(COO)}]$, obtained for **1-8** were in the range 202–236 cm^{-1} and indicated a monodentate coordination mode of the carboxylato group [20]. These changes in the IR spectra suggested that the fluoroquinolone ligands are bound to the metal ions via the ketone oxygen and a carboxylato oxygen. Complexes **2, 4, 6** & **8** exhibited characteristic strong bands for the pyridyl moiety ascribed to out-of-plane bending of the ring hydrogens in the range of 760-780 cm^{-1}, whereas the phenanthroline adducts **1, 3, 5** & **7** exhibits this band in the range of 725-775 cm^{-1}[21]. The complexes were 1:1 electrolytic in DMF, giving a molar conductance value of ~175 S cm^2M^{-1} at 25 °C.

The ESI-MS spectra of **1-8** showed molecular ion peaks at m/z 680.4 [M^+], 655.0 [M-1] (Fig. 4.2), 653.4 [M^+], 629.13 [M-1], 646.6[M-1], 626.6[M+3], 621.8 [M^+] and 597.6 [M^+] respectively. The m/z values of all complexes confirm the proposed

stoichiometry of the complexes which are in good agreement with that obtained from microanalytical data.

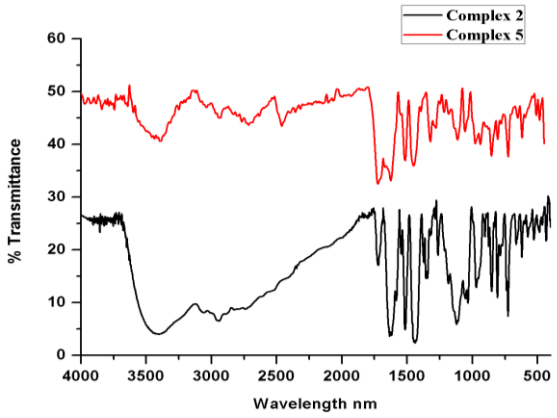

Fig 4.1: IR spectra of **2** and **5.**

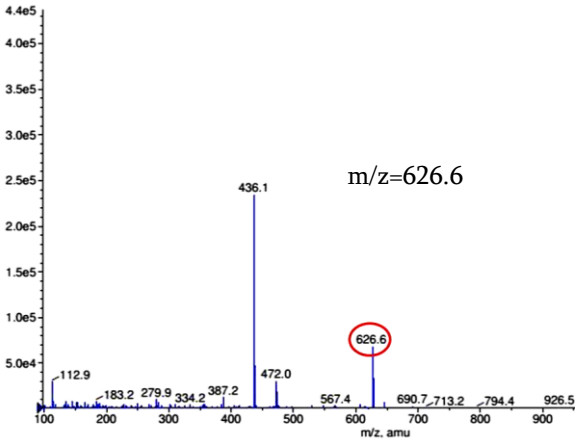

Fig 4.2: ESI-MS spectrum of Complex **6**.

Table 4.1: Characteristic IR bands (4000–400 cm^{-1}) of complexes **1-8.**

Compound	ν(C=O) pyridone	ν(C=O) carboxyl	ν(COO) asym	ν(COO) sym	Δ	ν(V=O)	SO_4 cm^{-1}	Bpy/ Phe
MFL	1712	1623	-	-	-	-	-	-
GFL	1731	1625	-	-	-	-	-	-
Complex 1	1627	-	1591	1386	205	-	-	775
Complex 2	1634	-	1587	1376	211	-	-	723
Complex 3	1684	-	1598	1385	213	-	-	775
Complex 4	1683	-	1589	1377	212	-	-	725
Complex 5	1632	-	1572	1370	202	954	1120	765
Complex 6	1627	-	1581	1365	216	964	1099	725
Complex 7	1624	-	1578	1342	236	950	1113	777
Complex 8	1635	-	1565	1328	237	962	1118	728

The electronic spectra of **1-8** in aqueous solution were recorded in the region 200-900 nm at room temperature. The electronic spectra of free MFL and GFL displayed intense absorption bands at ~290 and 330 nm respectively, which were shifted (Table

4.2) upon coordination with metal ions (Cu^{2+},VO^{2+}). These bands observed for **1-8** were attributed to $\pi \rightarrow \pi^*$ transitions of the fluoroquinolone ligands. The changes in the UV spectra of the complexes in comparison with that of free ligands were attributed coordination.

The electronic spectra of the **1–4** show in addition ligand-to-metal charge transfer transitions around ~420nm and broad absorption in the range 612-634 nm (ε =2.2 M^{-1} cm^{-1}) attributed to d–d transitions for Cu (II) in square pyramidal geometry [24]. In the visible region for **5-8**, two low-intensity bands at ~719-743 nm (band I), and 522-526nm (band II) attributed to d–d transitions are observed. Band I at λ~719-743 nm (ε = 7-17 M^{-1} cm^{-1}) is assigned to a b_2 (dxy) → e_π^*(dxz; dyz) transition and band II at λ ~522-526 nm to a b_2 (dxy) → $b_1^*(dx^2-y^2)$ transition of the VO^{2+} [22]. An intense third band at λ= 420-422 nm is observed which was attributed to ligand-to-metal charge-transfer transition. These bands were typical for square pyramidal VO^{2+} complexes [23].

Table 4.2: Electronic spectral data of complexes **1-8**.

Compound	Intraligand charge transfer transitions π-π*	CT Nm	d-d Transition nm
MFL	290, 330	-	-
GFL	287, 330	-	-
Complex 1	295, 370	410	634
Complex 2	296, 365	408	613
Complex 3	299, 360	420	638
Complex 4	300, 358	417	627
Complex 5	286, 337	437	522(Sh), 719
Complex 6	288, 337	435	522(Sh), 743
Complex 7	283, 332	408	526(Sh), 724
Complex 8	288, 330	402	526(Sh) ,748

The EPR spectra of copper and vanadyl complexes exhibit good hyperfine splitting and the corresponding $g_{\|}$, $g^{\perp}$ and $A_{\|}$ values are tabulated in Table 4.3. The analysis of low temperature X-band EPR spectra of **2** and **3** at 10 K in dmso is typical for

mononuclear Cu^{2+}complex in a square pyramidal geometry (Fig. 4.3(a)). Both the nitrogen adducts exhibit axial EPR spectra with g_{II} = 2.39, 2.48, $g_{\perp}$=2.0,2.1 and A_{II} values ranging from 134×10^{-4} cm $^{-1}$, 139×10^{-4} cm $^{-1}$. The lower $g_{\perp}$ values ($g_{II} > g_{\perp} >$ 2.0023) for **2** & **3** indicated that the unpaired electron of Cu (II) most likely resided in d_{x2-y2} orbital having $^2B_{1g}$ as ground state. The axial symmetry parameter (G=5.57) indicated that there are no spin exchange interactions between the copper centres (G>4) [24].

The spectra of vandyl complexes **6** and **7** exhibit a hyperfine eight-line pattern (Fig. 4.3 (a)), characteristic of an unpaired electron being coupled with a vanadium nuclear spin(I=7/2). The VO^{2+} ion belong to the $3d^1$ system and unpaired electron is in the vicinity of I=7/2 of its own mother nucleus. Thus, the spectra displayed well-resolved hyperfine lines and the signal parameters for complexes are given in table 4.3. The parallel component of the hyperfine coupling constant, $A_{//}$ is sensitive to the donor type in the "equatorial" coordination sphere. From this knowledge, the empirical additivity relationship has been developed and frequently used as a means of determining, to afirst approximation, the identity of the equatorial lignds in VO^{2+} vanadyl complexes [25]. On the basis of the additivity relationship, calculated $A_{//}$ ~159×10^{-4} cm $^{-1}$, with proposed equatorial coordination ($O_{carboxylate}$,O_{ketone} ,2 N_{Py}), where $A_{//}$(Ocarboxylate) = 42.7×10^{-4}cm^{-1},$A_{//}$ (O_{ketone})=38.9×10^{-4} cm $^{-1}$ and $A_{//}$(N_{py})= 39.0×10^{-4} cm $^{-1}$ [26], was close to the experimental $A_{//}$ = 170×10^{-4} value for the oxovanadium complexes. Thus, the most reasonable equatorial donor atom set was N_2O_2 for the oxovanadium complexes in the DMSO solution. The EPR hyperfine profile is similar to those of many other square pyramidal oxovanadium(IV) complexes reported earlier [27].

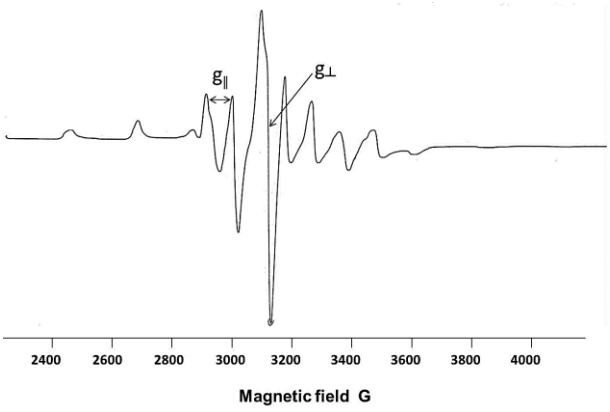

Fig 4.3: (a) ESR spectra of complex 6 in DMSO. EPR conditions: Temperature, 10K; microwave power, 5.0 mW; Modulation amplitude, 1G; microwave frequency, 9.1GHz.

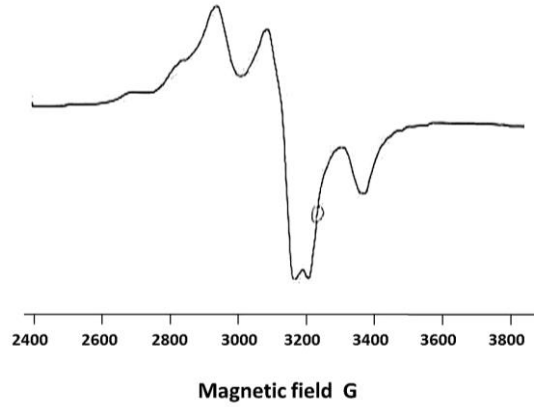

Fig 4.3: (b) ESR spectra of complex **2** in DMSO. EPR conditions: Temperature, 10K; microwave power, 5.0 mW; Modulation amplitude, 1G; microwave frequency, 9.1GHz.

Table 4.3: X-band ESR parameters of complex **2, 3, 6** and **7.**

Compound	$g_{\parallel}$	$g^{\perp}$	$g_{average}$	$A_{\parallel}$	$A^{\perp}$	G
Complex 2	2.39	2.0	2.19	134×10^{-4}	30.0×10^{-4}	5.3
Complex 3	2.48	2.1	2.29	139×10^{-4}	33.3×10^{-4}	4.8
Complex 6	2.12	2.09	2.1	169×10^{-4}	48.7×10^{-4}	5.3
Complex 7	2.06	1.90	1.98	170×10^{-4}	50.0×10^{-4}	4.6

The thermogravimetric analyses for the mixed-ligand complexes were carried out at temperature ranging from 20 to 800˚C in N_2 atmosphere at a rate of 10˚C per minute in order to establish their compositional differences as well as to ascertain the nature of associated water molecules. The TG curves of **1-4** shows three-decomposition steps (Fig. 4.4(a)), a loss in weight corresponding to five water molecules in the range of 50–130 °C indicates loss of water of crystallization, a second weight loss between 180–420 °C due to loss of the N-donor ligands, and a loss of weight between 440–690 °C due to loss of the ligand drugs MFL and GFL leaving behind CuO as a residue.

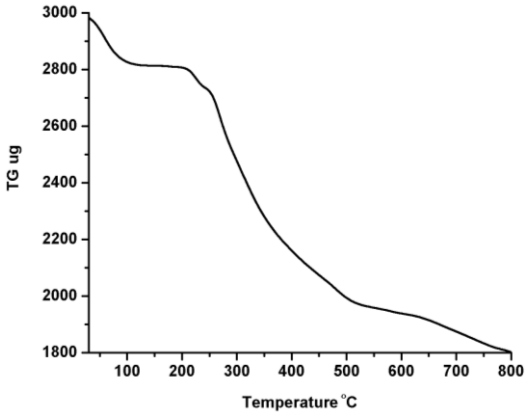

Fig 4.4: (a) Thermal degradation curve of the complex **2** at heating rate of 10 °C per minute under N_2 atmosphere.

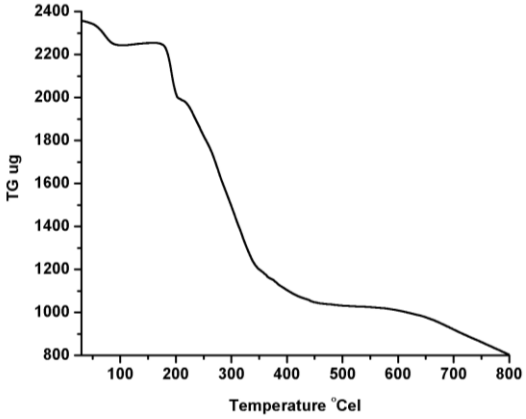

Fig 4.4: (b) Thermal degradation curve of the complex **6** at heating rate of 10 °C per minute under N_2 atmosphere

The temperature ranges and corresponding percent mass loss accompanying the changes in **5-8** on heating revealed the following (Fig.4.4(b)):

- Loss in weight corresponding to water of crystallization in the range of 50–130°C.
- Weight loss between 180–420 °C corresponding to the loss of the neutral ligand.
- Loss of weight during the final step, i.e. between 440–850 °C, due to loss of GFL and MFL, leaving behind metal oxide as a residue.

4.4.2 Antimicrobial Activity

A comparative study of zone inhibition values of the fluroquinolones and complexes **1-8** indicate that the metal complexes have better antibacterial activity than the fluroquinolones (Table 4.4). The inhibition activity seems to be governed to certain degree by the facility of coordination at the metal centre as well as bulkiness of the ancillary ligands.

The increased activity of complexes **1-8** compared to that of the free ligands may be explained in terms of chelation theory [28]. According to this theory, formation of the chelate rings enhance the lipophilicity of complexes, which breaks down the

permeability barrier of the cell retarding the normal cell processes. Antibacterial activity of ligands and complexes have been tested against two gram(-ve), E. coli, B.ptyphi and two gram(+ve), S. aureus and B. subtilis microorganisms. Results obtained reveal that all the tested 8 complexes possess potential antibacterial activity against B. subtilis & S. aureus. In general the increased antimicrobial activity of metal complexes may be explained by the chelate effect provided by both fluoroquinolones & N-donor ligand and the nature of the ligands.

Table 4.4: Zone of inhibition of MFL /GFL and their complexes **1-8** (1 µg/µL).

Compound	Gram (+ve)		Gram (-ve)	
	B. subtilis mm	*S. aureus* mm	*E. coli* Mm	*S. ptyphi* mm
MFL	15	13	12	14
GFL	17	15	14	14
Complex 1	24	22	21	20
Complex 2	25	23	17	19
Complex 3	27	28	21	16
Complex 4	29	24	18	17
Complex 5	28	25	24	23
Complex 6	28	23	23	20
Complex 7	27	29	18	19
Complex 8	26	25	16	16

4.4.3 DNA binding studies

4.4.3.1 UV-Visible absorption titration

We have used the absorption spectral technique to determine the mode of binding to CT DNA and intrinsic binding constants of the complexes by monitoring the absorption intensity of the charge transfer spectral bands 283-300 nm with increasing concentration of CT-DNA keeping the complex concentration constant. A complex bound to DNA through intercalation generally causes hypochromism and red shift (bathochromism) of the absorption band due to strong stacking interaction between the aromatic chromophore of the complex and the base pairs of DNA which reduces the energy of π-π* transitions and decreases transition probability [29].

The present complexes show hypo-chromism and red shift of the bands (~6 nm) due to strong stacking interactions indicating intercalating mode of binding (Fig 4.5).

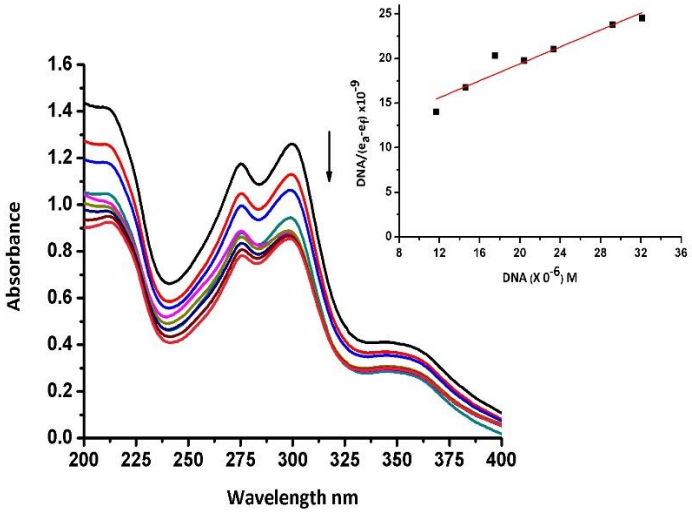

Fig 4.5: Absorption spectra of **2** (5μM)showing the decrease in absorption intensity on gradual addition of CT-DNA (0-35 μM) in 5 mM TrisHCl buffer (pH,7.2) at 25°C. Inset shows the plot of [DNA]/(ε_A-ε_f) vs [DNA].

The K_b values obtained for **1-8** from the absorption spectral technique are in the range 3.3-7.8 x10^6 M^{-1} (Table 4.5), suggested strong binding of the complexes to CT DNA through intercalation between aromatic chromophore of the ligands and DNA base pairs. The bpy complexes (**2, 4, 6** & **8**) showed lesser binding affinities to CT-DNA, while the phen analogues (**1, 3, 5** & **7**) are slightly better DNA binder compare to their bpy analouges.

4.4.3.2 Fluorescence quenching Studies

The binding of the complexes **1-8** to DNA through intercalation mode has further been verified by competitive fluorescence quenching experiments. The fluorescence spectra of EB-DNA complex ([EB] = 1×10^{-5}μM and [DNA] = 2.6×10^{-6} μM) in the absence and presence of **1-8** were recorded (Fig. 4.6) to confirm the intercalative mode of binding of the complexes with DNA. The addition of **1-8** in increasing amounts resulted in a significant decrease in the intensity of the emission band of the EB-DNA system at 610 nm indicating that the complexes displace EB from EB-DNA complex and interact with CT-DNA by intercalative mode. The Stern-Volmer plots (Fig 4.6, Inset) of EB-DNA system illustrate quenching of fluorescence by **1-8** in good agreement with the linear Stern-Volmer equation (eq 2.2), which indicate partial replacement of EB bound to DNA by each complex and resulting in decrease in the fluorescence intensity (Fig. 4.6(b)). The high K_{sv} values of the complexes (Table 4.5) reveal that the complexes strongly bind to CT-DNA by intercalation.

It might be concluded from the DNA binding studies that the binding of complexes with CT-DNA results mainly by the intercalation mode and the high binding affinity of the complexes towards CT-DNA as revealed by K_b and K_{sv} values could be due to presence of aromatic moieties in both the ligands which are known to show good DNA binding properties.

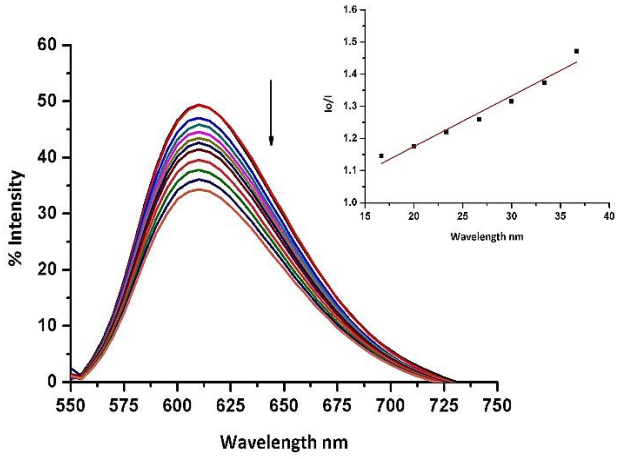

Fig 4.6: (a) The emission spectra of DNA bound EB in the presence of increasing concentration of complex **2** (0 -100 μM), DNA=26μM.
Inset Stern volmer plot Io/I vs Q (concentration),

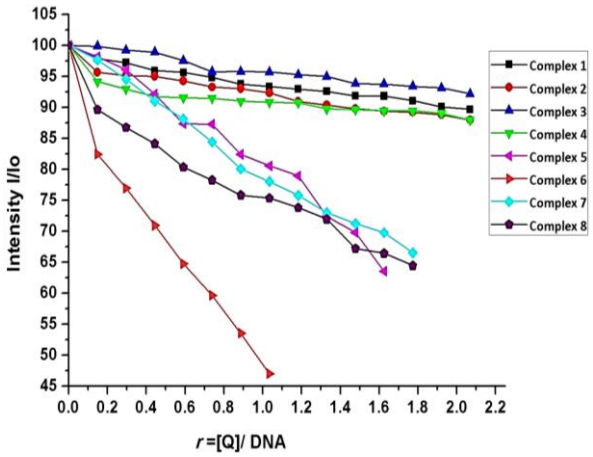

Fig 4.6: (b) Plot of EB–DNA relative Fluorescence intensity (% I/Io) at λ_{em}= 610 nm vs *r.*
(r = [compound Q] / [DNA]) in buffer solution (150 mM NaCl and 15 mM trisodium citrate at pH 7.0)

Table 4.5: DNA binding constants (K_b) and Stern–Volmer quenching constants (K_{SV}) of complexes **1–8.**

Compound	K_b	% Hypochromism	Red shift Nm	Ksv	% decrease in emission intensity of DNA-EB
MFL	1.0×10^5	10%	-	2.6×10^5	9%
GFL	2.0×10^4	12%	-	1.9×10^5	12%
Complex 1	5.2×10^6	17%	4	4.8×10^6	29%
Complex 2	4.0×10^6	28%	5	3.2×10^6	44%
Complex 3	7.8×10^6	24%	4	3.6×10^6	33%
Complex 4	3.5×10^6	31%	6	2.8×10^6	39%
Complex 5	4.7×10^6	26%	3	3.8×10^6	32%
Complex 6	3.3×10^6	39%	4	2.9×10^6	48%
Complex 7	5.9×10^6	27%	3	2.6×10^6	35%
Complex 8	3.9×10^6	37%	4	2.0×10^6	46%

4.4.3.3 Viscosity Measurements

Viscosity measurements were carried out to further verify the mode of interaction of the metal complexes with DNA. Changes in the viscosity of CT DNA in the presence of increasing amounts of the complexes **1–8** are given in Fig 4.7(a & b). It is observed that the viscosity of CT-DNA increased with increase in the concentration of complexes **1-8**. The increase in viscosity suggested that the complexes bind to DNA by intercalation.

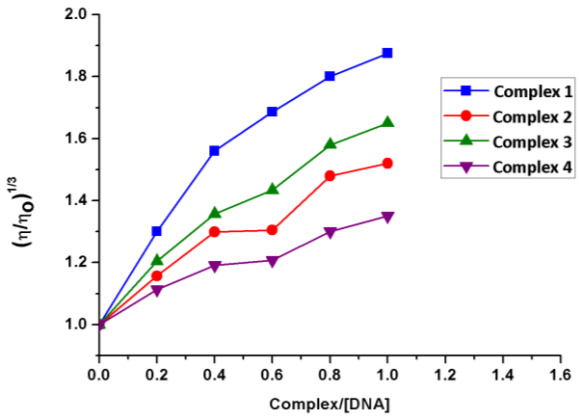

Fig 4.7(a) : The relative viscosity of DNA (50 μM) in the presence of complexes **1-4** (0 -60 μM) at 37.0 ºC in 5 mM Tris-HCl buffer (pH, 7.2).

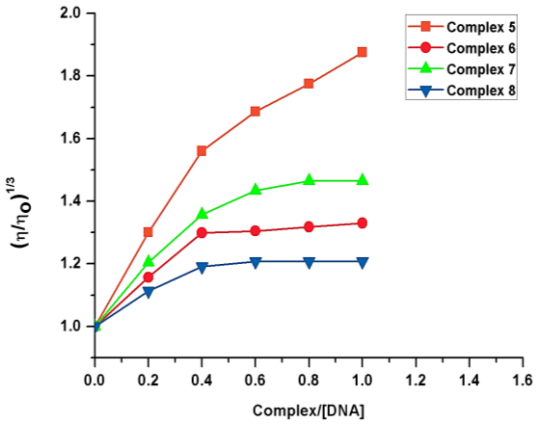

Fig 4.7(b) : The relative viscosity of DNA (50 μM) in the presence of complexes **5-8** (0-60 μM) at 37.0 ºC in 5 mM Tris-HCl buffer (pH,7.2).

4.4.3.4 Nuclease activity

Some of the anticancer agents approved for clinical use trigger cell death by damaging DNA [30], and the antitumor activities of several tested Cu(II) complexes [31] are in good correlation with the DNA cleavage activities. In order to explore the DNA cleavage abilities of the present complexes supercoiled (SC) pUC19 DNA (150 μM) was incubated with **1–8** (200 μM)in the absence of an activator in 5 mM Tris-HCl–50 mM NaCl buffer at pH 7.1 for 2 h at 37 °C. Interestingly, **7** and **8** caused double-strand DNA cleavage to generate the NC form (form III) before converting all of the SC form to OC DNA (form II) through single strand breaking,while **1–6** show single-strand

DNA cleavage to give only the OC form (Fig.3.8). The control experiments with the ligand or $CuCl_2 \cdot 6H2O$ /$VOSO_4.5H_2O$ or DNA alone did not reveal any significant cleavage. The effective DNA cleavage by the complexes was consistent with their high DNA affinities. The complexes did not require an external agent like ascorbic acid, MPA, or H_2O_2 for cleavage activity. DNA cleavage occured via oxidative pathway.

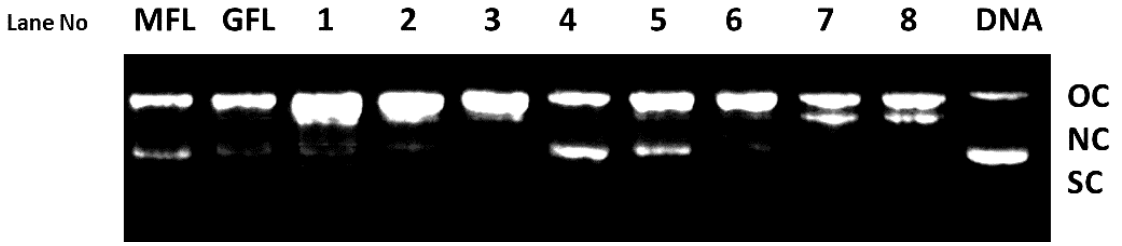

Fig 3.8 : Photogenic view of interaction of pUC19 DNA (150 μg/mL) with 200 μM complexes incubated for 2hours at 37 °C: Lane 1, **MFL**; Lane 2, **GFL**; Lane 3, DNA + **1**; Lane 4, DNA + **2**; Lane 5, DNA + **3**; Lane 6, DNA + **4**; Lane 7, DNA +**5**; Lane 8, DNA +**6**; Lane 9, DNA +**7**; Lane **10**, DNA +**8** ; Lane 10, DNA control.

4.4.4 Interaction with Proteins

4.5.4.1 Protein binding

The binding affinity of **1–8** to the bovine serum albumin (BSA) protein was studied with the aid of tryptophan emission quenching techniques. The emission of BSA occurs due to the presence of the tryptophan residues, namely, trp-134 and trp-212. Upon the addition of **1–8** the emission intensity of BSA is found to decrease revealing that changes in the protein secondary structure as well as the tryptophan environment of BSA occured upon the binding of the complexes (Fig. 4.9). The extent of quenching of the fluorescence intensity, as expressed by the value of the Stern–Volmer constant (Ksv), is considered to be a measure of the protein binding affinity of the complexes [32]. The Ksv values is obtained as the slope of the linear plot of I_0/I vs. [complex]. The calculated values of Ksv (quenching constant) in the range 4.2-8.6 x 10^6 M^{-1}, indicat good BSA binding propensity of the complexes, with **4** exhibiting the strongest protein-binding ability (Table 4.6).

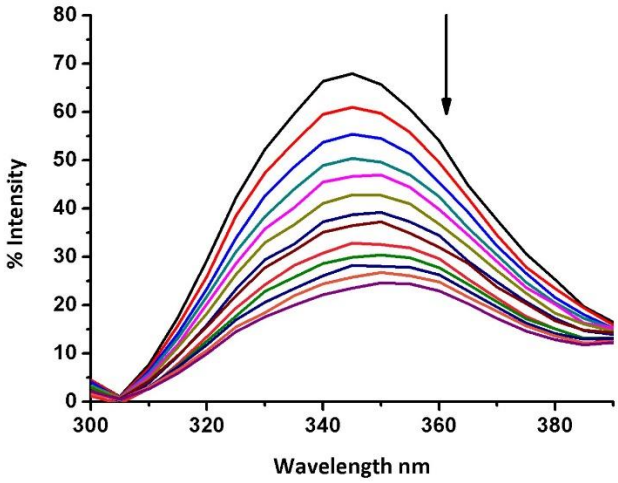

Fig 4.9: Emission spectra of BSA (6.6 μM) in presence of complex **3** (0-10 μM) in tris buffer at 37˚C.

Table 4.6: Quenching constant Ksv, for the interaction of Complexes **1-8** with BSA.

Complex	**1**	**2**	**3**	**4**	**5**	**6**	**7**	**8**
Ksv x10^6 M^{-1}	4.2	6.2	5.0	8.6	4.7	5.6	4.2	6.5

4.5.4.2 Protein cleavage studies

Designing an enzyme-like catalyst for the hydrolysis of peptide bonds of a protein is challenging in view of their high stability. Biochemical procedures involved in protein sequencing, foot printing and folding studies require the partial degradation of proteins via the regioselective hydrolysis of peptide bonds. The ability of **1–8** to cleave protein peptide bonds is studied using BSA as a substrate. In the absence of an activator like ascorbic acid and hydrogen peroxide, no protein cleavage is observed (Fig. 4.10(a)). When the protein (5μM) was incubated at 50 °C (Fig. 10b) with **1–4** (500μM) in the presence of H_2O_2 (500 μM) at pH 7.2 and then subjected to SDS-PAGE, all the synthesized complexes showed protein cleavage compared with the untreated BSA control band (Fig. 10 b). Significant smearing or fading of the BSA band in the presence of **1-8** suggested non-specific binding to BSA. When the hydroxyl radical scavenger DMSO was added to the reaction mixture, inhibition of BSA cleavage is observed revealing the involvement of the •OH radicals in the cleavage reaction. Thus, **1-8** bind to protein and generate ROS species, which in turn are involved in protein cleavage.

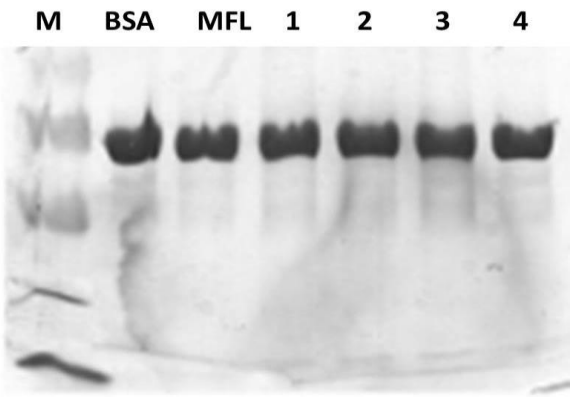

Fig 4.10 (a): 12.5% SDS-PAGE diagram showing the cleavage of BSA (5 μM) in the presence of **1-4** with an exposure time of 30 min in 50 mM Tris-HCl buffer (pH 7.2): Lane 1, molecular marker; lane 2, BSA control; lane **3**, BSA + **1**; lane 4, BSA + **2** ; lane 5, BSA + **3**; lane 6, BSA + **4** .

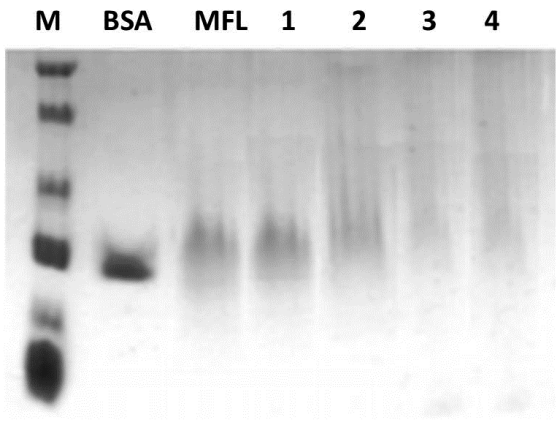

Fig 4.10 (b): 12.5% SDS-PAGE diagram showing the cleavage of BSA (5 μM) in the complexes **1-4** with an exposure time of 30 min in 50 mM Tris-HCl buffer (pH 7.2): Lane 1, molecular marker; lane 2, BSA control; lane 3, BSA + **1**+H_2O_2; lane 4, BSA + **2**+ H_2O_2 ; lane 5, BSA + **3**+ H_2O_2; lane 6, BSA + **4** +H_2O_2 .

4.4.5 Cytotoxicity studies

4.4.5.1 MTT assay

The cytotoxicity of complexes **1–8** was determined using MTT assay [33] on A549 human lung cancer cells by treating them with the compounds at varying concentrations (5–95 μg/ml) for 12h. All the complexes inhibited the growth of lung cancer cells significantly in a dose and time dependent manner and recorded 50–85% higher cytotoxicity compared to the fluoroquinolone drugs. The IC_{50} values are shown in Fig. 4.11 which indicate the order of cytotoxicity as **6**<**8**<**4**<**2**<**5**<**7**<**3**<**1**.The results reveal enhancement in the antiproliferative activity of the parent quinolone ligand (MFL/GFL) upon metal (Cu^{2+}/VO^{2+}) conjugation giving credence to the hypothesis that biological activity of such quinolones may partly be related to their metal chelating ability. Amongst the compounds examined presently, the copper phenanthroline adduct was found to be the most potent molecule. Based on our earlier work on metal-quinolonates we would like to suggest that the facile Cu^{+2}/Cu^{+1} redox couple may act as redox trigger for activating apoptotic processess. This observation could pave way for generating more robust biologically active metal-fluoroquinolonate complexes as drugs.

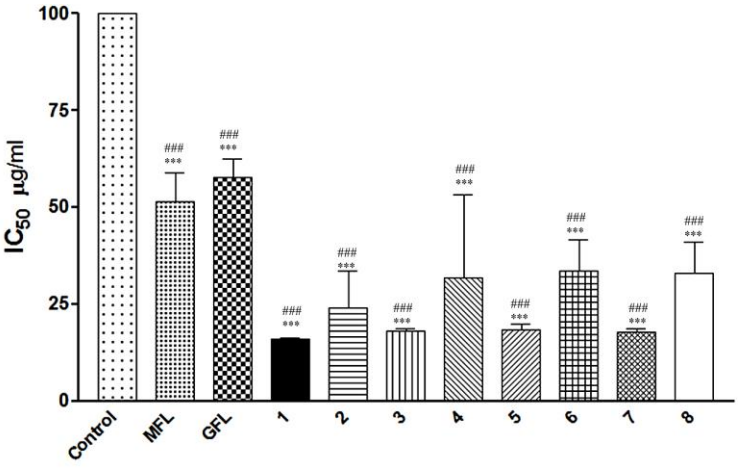

Fig 4.11: Data expressed as mean ±S.E.M. for n=3.
Where, ***p<0.001 compared to GFL and ###p<0.001 compared to MFL. 50% inhibition concentration (IC_{50} μg/ml) for complexes **1–8.**

4.4.5.2 Alterations in cell morphology

To further investigate the cytotoxicity of complexes **1-8** on A549 cells, we determined the effect of the complexes on the morphology of these cells by light microscopy. A549 cells showed fibroblastic characteristics with very well stained cytoplasm, spindle shape, adherent nature and oval nuclei. On treatment with complexes majority of the cells were rounded in appearance and showed cell surface blebbing, an early feature of apoptosis (Fig. 4.12). Some cells became irregular in shape and size with altered nuclear: cytoplasmic ratios and had relatively flattened appearance (Fig. 4.12) indicating that these drugs induced some changes in cell surface associated with the adherence to the substratum. Appearance of multinucleated giant cells suggesting inhibition of cytokinesis was also observed.

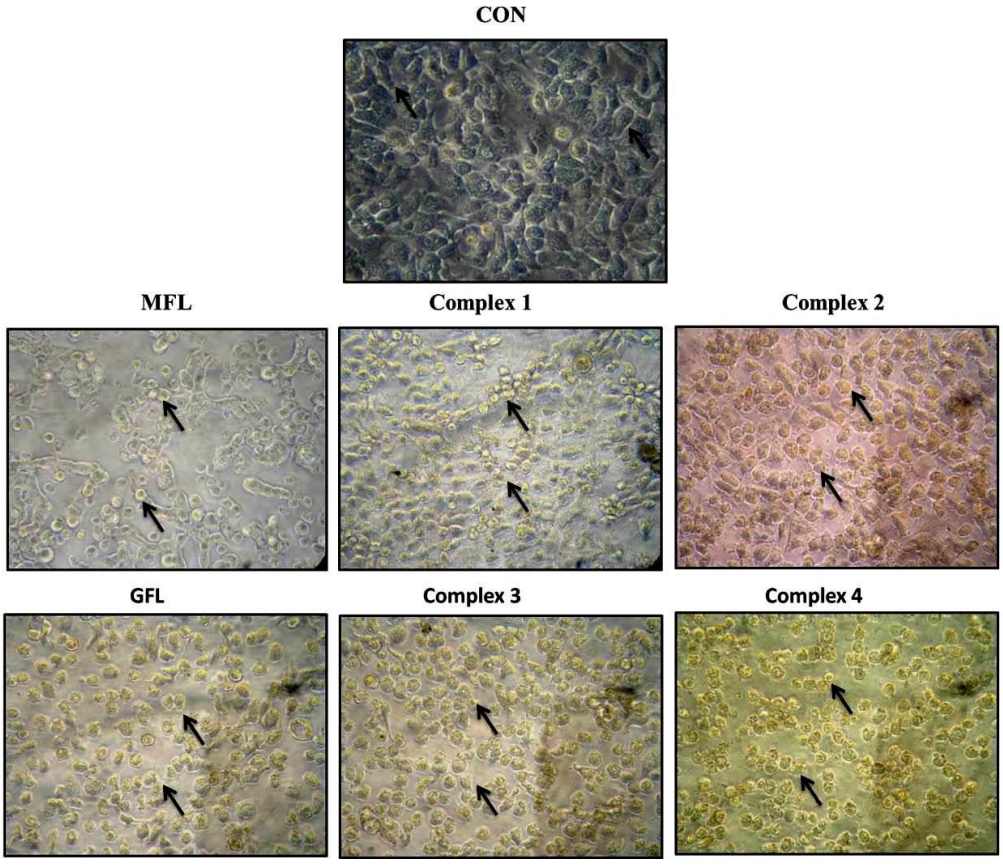

Fig 4.12: A-549 cells observed under phase-contrast microscope before and after treatment with complexes **1-4.**

4.4.5.3 Assessment of mode of cell death based on morphological features (AO/EB staining)

Cell death is divided into two types, necrosis and apoptosis. Necrosis causes inflammation while apoptosis does not. Induction of tumor cell apoptosis has already been used as an important indicator to detect the ability of chemotherapeutic drugs to inhibit tumor growth [34]. We have studied the mode of cell death induced by **1–8** by adopting fluorescent staining for morphological assessment of cell death.A549 cells treated with **1–8** (18.1μg/ml) stained with AO/EB exhibited morphological changes typical of apoptosis including cell shrinkage, plasma membrane blebbing, chromatin condensation and nuclear fragmentation as compared to control cells with prominent rounded nuclei and defined plasma membrane contours. From the results (Fig. 4.13), we found that maximum number of late apoptotic cells were seen in the presence of all the complexes. These morphological changes suggested that the mode of cell death was apoptotsis induced by **1-8**.

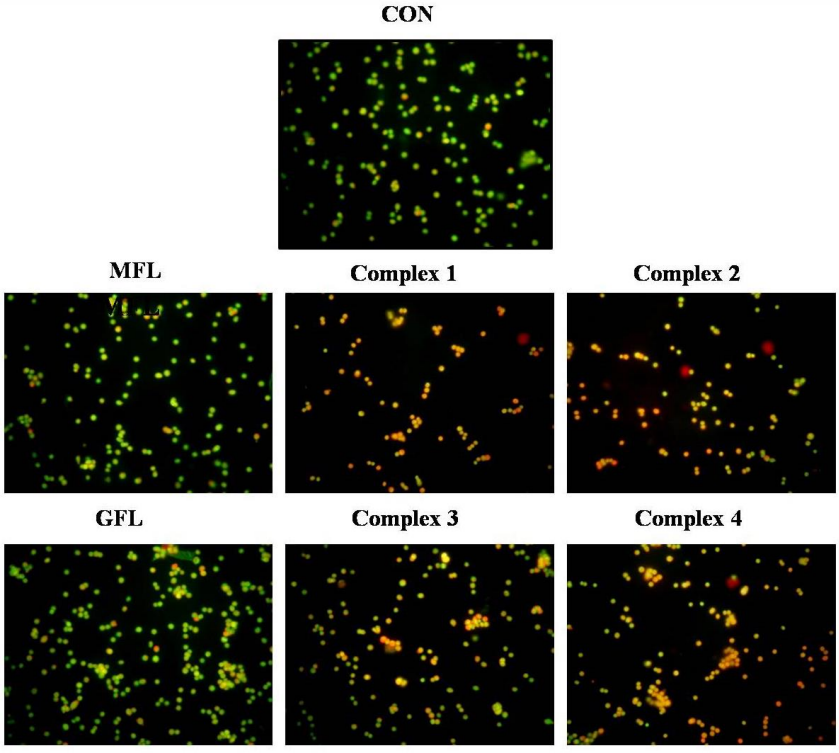

Fig 4.13: A549 cells were stained by AO/EB and observed under fluorescence microscope: (a) A549 cell without treatment (CON) (b) in the presence of MFL (c) in the presence of complex **1** (d) in the presence of complex, **2** (e) in the presence of **GFL** (f) in the presence of complex, **3** (g) in the presence of complex, **4** incubated at 37 °C and 5% CO_2 for 12 h.

4.4.5.4 Dapi Staining

The molecular mechanism of cell death has been studied by treating the A549 lung cancer cells with IC_{50} concentrations of **1–8** for 12 h and then observing them for cytological changes by adopting Dapi staining. The representative morphological changes observed for **1–8** such as chromatin fragmentation, bi-and/or multinucleation, cytoplasmic blebbing and late apoptosis indication of dot-like chromatin condensation [35] are shown in Fig. 4.14. Also, the number of abnormal cells was found to increase with the incubation time revealing that all of the complexes caused cytological changes in a time dependent manner. The apoptosis-inducing abilities of complexes were consistent with the hydrophobicity of the ligands, which facilitated the transport of the complexes across the cell membrane and their eventual release at various organelles to bind with DNA leading to apoptosis, which accounted for their higher cytotoxicity.

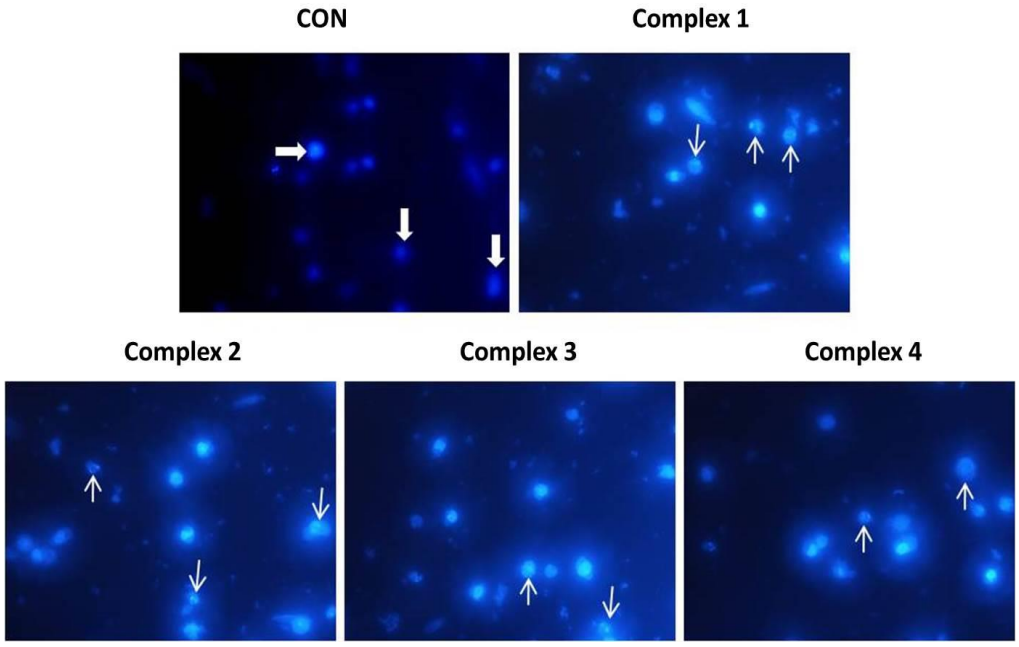

Fig 4.14: Micropotographs of A549 cells were stained by DAPI and observed under fluorescence microscope: (a) A549 cell without treatment (CON); in the presence of (b) **1**; (c) **2**; (d) **3** ; (e) **4** ; incubated at 37 °C and 5% CO_2 for 12 h..

4.4.5.5 Intracellular ROS generation and oxidative stress

ROS are not only cytotoxic by-products that trigger cell death through oxidative damage, but can also act as signaling molecules targeting specific components of metabolic and signal transduction pathways [36]. ROS levels were evaluated by fluorescence spectroscopy using DCFDA as a probe. To study whether the cell death induced by complexes **1-8** is dependent on ROS generation, A549 cells were treated with complexes (IC_{50}) for 6-12 h and then stained with DCFDA. The dichlorofluorescein fluorescence intensity of dichlorofluorescein increased significantly with time in cells treated with **1-8** compared to that of control as shown in Fig.4.15. Moreover, the fluorescence intensity was concentration-dependent. These results indicated that **1-8** enhance the level of intracellular ROS.

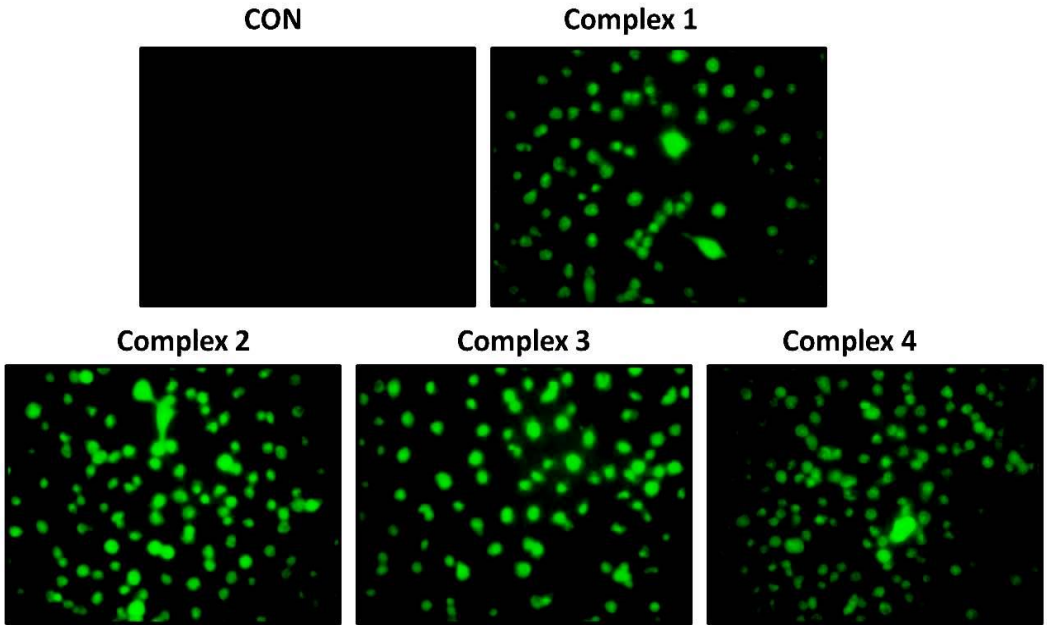

Fig 4.15: Micropotographs of A549 cells were stained by DCFDA and observed under fluorescence microscope: (a) A549 cell without treatment (CON); in the presence of (b) **1**; (c) **2**; (d) **3** ; (e) **4** ; incubated at 37 °C and 5% CO_2 for 12 h.

4.4.5.6 Assessment of DNA damage

Apoptosis is a physiologically gene-directed programmed cell death mechanism that regulates cell homeostasis and plays a crucial role in the proliferation and turnover of cells in a variety of tumors and cancer cells. Applying Eastmans protocol [37], we investigated induction of apoptosis by complexes **1-8** of A549 cells at different time points. The results presented in Fig. 4.16 show that MFL/GFL does provoke DNA fragmentation in A549 cells, but the phenomenon was very weak and took place only after 48 h incubation with the drugs. In contrast 1-**8** caused typical fragmentation of the DNA of the cell nucleus in 320 bp fragments, i.e., complexes induce apoptosis after 16 h incubation (Fig. 4.16) without significant necrotic effects, implying that coordination with metal ions enhanced the apoptotic effect of the drug (MFL/GFL) in A549 cells. Taking in account all the *in vitro* cytotoxicity studies and DNA cleavage experiments, the mechanism of action of the complexes appeared to be via a free radical pathway.

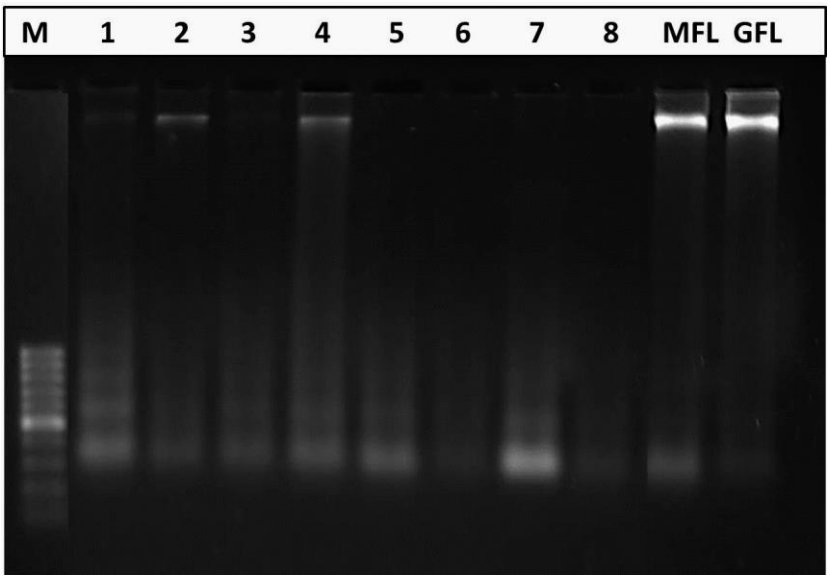

Fig 4.16: Photogenic view of cleavage of A-549 cells with series of complexes 1-8 using 1.5% agarose gel containing ethidium bromide. All complexes were incubated for 16 h at 37 °C. Lane 1, Marker M; Lane 2, complex **1**; Lane 3, complex **2**; Lane 4, complex **3**; Lane 5, complex **4**; Lane 6, complex **5**; Lane 7, complex **6**; Lane 8, complex **7**; Lane 9, complex **8**; Lane 10, MFL; Lane 11,GFL.

4.5 Conclusion

In this chapter, we have studied interaction of mixed ligand Cu(II)/VO(II) complexes with nucleic acids and analyzed their biochemical effect on human lung cancer cells. Synthesis and characterization of eight mononuclear copper(II)/vanadyl(II) complexes with fluoroquinolone drugs (GFL & MFL) in the presence of nitrogen-donor heterocyclic ligands (phen&bpy) have been realized with physicochemical and spectroscopic methods. In all the complexes, the quinolone ligand was bound to metal ion via the pyridone oxygen and one carboxylate oxygen. For all the complexes, a distorted square pyramidal environment around metal centre has been suggested.

All the complexes were found to be involved in intercalation into the DNA base pairs. Along with the spectroscopic techniques the proposed mode of DNA binding was supported by the enhancement in relative viscosity of DNA upon binding to the complexes. Complexes **1-8** could induce scission of PUC19 supercoiled DNA effectively without addition of external agents at pH =7.2 and 37 °C. The strong DNA binding ability coupled with the potent DNA cleavage activity revealed that the complexes promote DNA cleavage through an oxidative DNA damage pathway. Interestingly, the complexes also showed higher affinity to bind to BSA protein in the hydrophobic region and ability to cleave it in the presence of a reductant. **1-8** prefer to bind to protein and generated ROS species, which in turn was involved in protein cleavage.

The antimicrobial activity of the complexes was been tested on four different microorganisms and the results have showed an enhanced antibacterial activity in comparison to the free quinolone ligands, while the nature of the N-donor ligands might have facilitated antibacterial activity. The best inhibition among the compounds studied in this work is provided by phenanthroline adducts against gram-ve bacteria. Remarkably all the complexes displayed cytotoxicity against human lung cancer (A549) cell lines higher than the fluoroquinolones (MFL/GFL) and metal-phen

adducts with enhanced hydrophobicity exhibited higher cytotoxicity. Further all the complexes showed effective cell growth inhibition by generating ROS and inducing apoptosis. Our data here suggested that the complexes could be good antitumor drugs and a practical probe of DNA sequence. The complexes are projected to be potential anticancer molecules that may interfere with DNA replication where the intercalation is the preferred binding mode. Additionally, the experimental results confirmed the strong binding to DNA, which can help to promote novel rational design of drugs for chemotherapy.

References

[1] L.A. Summers, Adv. Heterocycl. Chem., 22 (1978) 1.

[2] P.G. Sammes, G. Yahioglu, Chem. Soc. Rev., 23 (1994) 327.

[3] G. Christian Kaes , A. Katz , and Mir Wais Hosseini, Chem. Rev., 100 (2000) 3553.

[4] R. Ziessel, L. Toupet, S. Chardon-Noblat, A. Deronzier, D.J. Matt, Dalton Trans., (1997) 3777.

[5] K.E. Erkkila, D.T. Odom, J.K. Barton, Chem. Rev., 99 (1999) 2777.

[6] D.S. Sigman, R. Landgraf, D.M. Perrin, L. Pearson, in: A. Sigel, H. Sigel (Eds.),

[7] R.R. Crichton, Biological Inorganic Chemistry: an introduction, Elsevier, Amsterdam, 2008.

[8] D.S. Sigman, D.R. Graham, V. D'Aurora, A.M. Stern, J. Biol. Chem., 254 (1979) 12269.

[9] A. Serafin, A. Stańczak, Russ. J. Coord. Chem., 35 (2009) 81.

[10] M.E. Katsarou, E.K. Efthimiadou, G. Psomas, A. Karaliota, D. Vourloumis, J. Med. Chem., 51 (2008) 470.

[11] J.O. Nriagu, Vanadium in the Environment, Part 2, Health Effects, John Wiley & Sons, New York, 1998.

[12] D. Rehder, Bioinorganic Vanadium Chemistry, John Wiley & Sons, New York, 2008.

[13] D. Rehder, Inorg. Chem. Commun., 6 (2003) 604.

[14] B.V. Venkataraman, S. Sudha, Asian J. Exp. Sci.,19 (2005) 127.

[15] A.M. Cortizo, S.B. Etcheverry, Mol. Cell. Biochem., 145 (1995) 97.

[16] V.C. Sálice, A.M. Cortizo, C.L. Gómez Dumm, S.B. Etcheverry, Mol. Cell. Biochem., 198(1999) 119.

[17] I.E. León, A.L. Di Virgilio, D.A. Barrio, G. Arrambide, D. Gambino, S.B. Etcheverry, Metallomic., 4 (2012) 1287.

[18] A. Sreedhara, N. Susa, A. Patwardhan, C.P. Rao, Biochem. Biophys. Res. Commun., 35(1996) 79.

[19] J.H. McNeill, V.G. Yuen, H.R. Hoveyda, C. Orvig, J. Med. Chem., 35 (1992) 1489.

[20] Y.Shechter, A.Shisheva, R.Lazar, J.Libman, A.Shanzer, Biochem., 31(1992) 2063.

[21] S. Rajabalian, A. Foroumadi, A. Shafiee, S. Emami, J Pharm Pharmaceut Sci., 10 (2) (2007) 153.

[22] C. Herold, M. Ocker, M. Ganslmayer, H. Gerauer, E.G.Hahn, D. Schuppan, Br.J.Cancer., 86 (2002) 443.

[23] E. J. Tolis, V. I. Teberekidis, C. P. Raptopoulou, A.Terzis, M.P. Sigalas, Y. Deligiannakis, T. A. Kabanos, Chem. Eur. J., 7 (2001) 2698.

[24] H. Kelm, H.J. Kruger, Inorg. Chem., 35 (1996) 3533.

[25] O. Aranha, R. Grignon, N. Fernandes, T. J. McDonnell, D. P. Wood, F. H. Sarkar, Int. J. Oncol., 22 (2003) 787.

[26] N.D. Chasteen, in: J. Lawrence, L.J. Berliner, J. Reuben (Eds.), Biological Magnetic Resonance, vol. 3, Plenum, New York, 1981, pp. 53.

[27] G. Micera, V.L. Pecoraro, E. Garribba, Inorg. Chem., 48 (2009) 5790.

[28] M. Mathieu, P. Van Der Voort, B.M. Weckhuysen, R.R. Rao, G. Catana, R.A. Schoonheydt, E.F. Vansant, J. Phys. Chem., B 105 (2001) 3393.

[29] B.M. Zeglis, V.C. Pierre, J.K. Barton, Chem. Commun., (2007) 4565.

[30] L. E. Gunther, A. S. Yong, J. Am. Chem. Soc., 90 (1968) 7323.

[31] A. Natrajan and S. M. Hecht, , ed. S. Neidle and M. Waring, CRC Press, Boca Raton, FL, 1994, vol. 2, p. 197.

[32] V. Rajendiran, R. Karthik, M. Palaniandavar, H. S. Evans, V. S. Periasamy, M. A. Akbarsha, B. S. Srinag and H. Krishnamurthy, Inorg. Chem., 46 (2007) 8208.

[33] C. V. Kumar, A. Buranaprapuk, H. C. Sze, S. Jockusch and N. J. Turro, Proc. Natl. Acad. Sci. U. S. A., 99 (2002) 5810.

[34] M. T. Garland, J. Y. Le Marouille and E. Spodine, Acta Crystallogr., Sect. C: Cryst. Struct. Commun., 42 (1986) 1518.

[35] T. Zhang, X. Chen, L. Qu, J. Wu, R. Cui, Y. Zhao, Bioorg. Med. Chem., 12 (2004) 6097.

[36] J. Gao, Y.-G. Liu, Y. Zhou, L.M. Boxer, F.R. Woolley, R.A. Zingaro, Chem Bio Chem., 8 (2007) 332.

[37] E. Junn, K.N. Lee, H.R. Ju, S.H. Han, J.Y. Im, H.S Kang, T.H. Lee, Y.S. Bae, K.S. Ha, Z.W. Lee, S.G. Rhee, I. Choi, J Immunol., 165(2000) 2190.

[38] A. Eastman, Meth. Cell Biol., 46 (1995) 41.